The proton charge radius extracted from the Initial State Radiation experiment at MAMI

M. Mihovilovič[a,b,c], P. Achenbach[c], T. Beranek[c], J. Beričič[b], J. C. Bernauer[d], R. Böhm[c], D. Bosnar[e], M. Cardinali[c], L. Correa[f], L. Debenjak[b], A. Denig[c], M. O. Distler[c], A. Esser[c], M. I. Ferretti Bondy[c], H. Fonvieille[f], J. M. Friedrich[g], I. Friščić[d], K. Griffioen[h], M. Hoek[c], S. Kegel[c], H. Merkel[c,*], D. G. Middleton[c], U. Müller[c], J. Pochodzalla[c], B. S. Schlimme[c], M. Schoth[c], F. Schulz[c], C. Sfienti[c], S. Širca[a,b], S. Štajner[b], Y. Stöttinger[c], M. Thiel[c], A. Tyukin[c], M. Vanderhaeghen[c], A. B. Weber[c]

[a] *Faculty of Mathematics and Physics, University of Ljubljana, SI-1000 Ljubljana, Slovenia*
[b] *Jožef Stefan Institute, SI-1000 Ljubljana, Slovenia*
[c] *Institut für Kernphysik, Johannes Gutenberg-Universität Mainz, DE-55128 Mainz, Germany*
[d] *Massachusetts Institute of Technology, Cambridge, MA 02139, USA*
[e] *Department of Physics, Faculty of Science, University of Zagreb, HR-10002 Zagreb, Croatia*
[f] *Université Clermont Auvergne, CNRS/IN2P3, LPC, BP 10448, F-63000 Clermont-Ferrand, France*
[g] *Technische Universität München, Physik Department, 85748 Garching, Germany*
[h] *College of William and Mary, Williamsburg, VA 23187, USA*

Abstract

We report on a comprehensive reinterpretation of the existing cross-section data for elastic electron-proton scattering obtained by the initial-state radiation technique, resulting in a significantly improved accuracy of the extracted proton charge radius. By refining the external energy corrections we have achieved an outstanding description of the radiative tail, essential for a detailed investigation of the proton finite-size effects on the measured cross-sections. This development, together with a novel framework for determining the radius, based on a regression analysis of the cross-sections employing a polynomial model for the form factor, led us to a new value for the charge radius, which is $(0.873 \pm 0.011_{\text{stat.}} \pm 0.025_{\text{sys.}} \pm 0.003_{\text{mod.}})$ fm.

Keywords: Initial state radiation, Proton radius, Radiative corrections
PACS: 12.20.-m, 25.30.Bf, 41.60.-m

1. Introduction

The problem of the proton charge radius arose from the significant deviation of the very precise Lamb shift measurements in muonic hydrogen [1, 2], which gave a value of 0.84087(39) fm from the CODATA[3] value of 0.8751(61) fm, compiled from electron scattering, and the old atomic Lamb shift measurements. This discrepancy has motivated several follow-up measurements, but despite the efforts remains unresolved. While the measurement of the $2S$-$4P$ transition in Hydrogen [4] and the new scattering experiment at Jefferson Lab [5] yield values of 0.8335(95) fm and 0.831(14) fm, which are in agreement with the smaller radius, the measurement of the $1S$-$3S$ transition [6] gives a value of 0.877(13) fm, and supports the hypothesis of a large proton radius. Therefore, additional experiments, both scattering and spectroscopic, have the potential to make valuable contributions to the proton size problem [7, 8].

In scattering experiments the charge radius of the proton is traditionally determined by measuring the cross section for elastic scattering of electrons from hydrogen, which depends on G_E^p and carries information about the charge distribution of the proton. The proton charge radius, r_p, is given by

$$r_p^2 \equiv -6\hbar^2 \frac{\mathrm{d}G_E^p}{\mathrm{d}Q^2}\bigg|_{Q^2=0}, \tag{1}$$

where Q^2 is the negative square of the four-momentum transfer to the proton. The accuracy of the radius obtained in this manner is limited by the extent of available data sets, which dictates the approach to the extrapolation of G_E^p needed to determine the slope at $Q^2 = 0$. Hence, to ensure reliable extraction of the radius, measurements of G_E^p are needed in the region of $Q^2 \lesssim 0.01\,\mathrm{GeV}^2/c^2$.

Efforts to perform such measurements with the standard approaches are limited by the minimum Q^2 accessible with the experimental apparatus at hand, predominantly due to the restrictions in the available electron beam energy and the minimum scattering angle. Therefore, a new experimental approach based on initial state radiation has been introduced [10] that allows for cross section measurements down to $0.001\,\mathrm{GeV}^2/c^2$ with subpercent precision by using information about the charge form factor that is implicit in the radiative tail of the elastic peak.

2. Initial-state radiation experiment

The radiative tail of an elastic peak is dominated by the coherent sum of two Bethe-Heitler diagrams [9] shown in Figure 1. The initial state radiation diagram (BH-i) describes the

*Corresponding author
Email address: merkel@kph.uni-mainz.de (H. Merkel)

process where the incident electron emits a real photon before interacting with the proton. Since the emitted photon carries away a fraction of the incident energy, the momentum transfer to the proton is decreased. Hence, this process probes the proton structure at values of Q^2 smaller than the value fixed by the experimental kinematics and is thus sensitive to the form-factors at Q^2 smaller than those corresponding to the elastic setting. On the other hand, the final state radiation diagram (BH-f) corresponds to the reaction where the real photon is emitted after the interaction with the nucleon. Consequently, Q^2 at the vertex remains constant, while the detected four-momentum transfer changes.

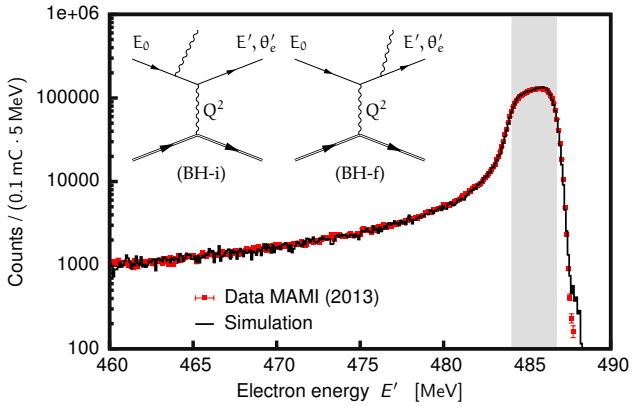

Figure 1: Measured and simulated elastic peak with the corresponding radiative tail for the first kinematic setting at 495 MeV. See [10] for details. The radiative tail is dominated by the two Bethe-Heitler diagrams (BH-i and BH-f), where electrons emit real photons before or after the interaction with the protons. The grey band marks the position and width of the elastic line inside the spectrometer acceptance.

In an inclusive experiment Q^2 can not be measured directly, which means that looking only at the data the initial state radiation processes can not be distinguished from the final state radiation. Hence, in order to get information on G_E^p at Q^2 smaller than the elastic setting, the data must be studied in conjunction with a Monte-Carlo simulation, which includes a detailed description of the radiative corrections and considers G_E^p as its free parameter. This is the basic idea of the MAMI experiment, which opened the door of obtaining G_E^p down to $Q^2 \simeq 10^{-4}\,\mathrm{GeV}^2/c^2$ [10].

The measurement of the radiative tail has been performed at the Mainz Microtron (MAMI) in 2013 using the spectrometer setup of the A1-Collaboration [11]. A rastered electron beam with energies of E_0 = 195, 330 and 495 MeV was used in combination with a hydrogen target, which consisted of a 5 cm-long cigar-shaped Havar cell filled with liquid hydrogen and placed in an evacuated scattering chamber. For the cross section measurements the single-dipole magnetic spectrometer B was employed at a fixed angle of 15.21°, while its momentum settings were adjusted to scan the complete radiative tail for each beam energy. The central momentum of each setting was measured with an NMR probe to a relative accuracy of 8×10^{-5}. The spectrometer was equipped with the standard detector package consisting of two layers of vertical drift chambers (VDCs) for tracking, two layers of scintillation detectors for triggering, and a threshold Cherenkov detector for particle identification. The kinematic settings of the experiment were chosen such that the radiative tails scanned at three beam energies overlap.

The beam current was between 10 nA and 1 μA and was limited by the maximum rate allowed in the VDCs ($\approx$ 1 kHz/wire), resulting in raw rates up to 20 kHz. The beam current was determined by a non-invasive fluxgate-magnetometer and from the collected charge of the beam stopped in a Faraday cup. At low beam currents and low beam energies the accuracy of both approaches is not better than 2 %, which is insufficient for precise cross section measurements. Hence Spectrometer A was used at a fixed momentum and angular setting for precise monitoring of the relative luminosity.

The analysis of the data, presented in [10], revealed inconsistencies between data and simulation on the order of 10 % at the top of the elastic peak, see Fig. 2, which led to the omission of the most statistically relevant, elastic data points in the sample. The inconsistency arose due to the incomplete correction for the electron energy losses in the target material. To be able to incorporate the elastic data in the analysis and ensure a more precise extraction of the proton charge radius, the estimations of the external corrections had been investigated in detail.

The external radiative corrections were considered using the formalism of Mo and Tsai [12], while the collisional corrections were approximated by the Landau distribution [13]. The uncertainty of the applied energy corrections was estimated to be smaller than 1 % [12]. This was confirmed by the dedicated followup experiment, using the same experimental setup but different targets. Data were collected using plastic ($[CH_2]_n$) targets with different thicknesses, which created a perfect testbed for validating the applied corrections, since the spectra differ only in the size of the external energy loss correction. The comparison of the elastic peak shapes for different target thicknesses with the simulations presented the correct scaling of the corrections with the thickness of the target.

The impact of the external radiative and collisional corrections on the shape of the radiative tail is observable only in first few MeV of the radiative tail, see Fig. 2. Hence, an inconsistency between the data and simulation in this region is an indication of an unaccounted for material traversed by the electrons. These inconsistencies are related to the traces of cryogenic deposits on the end caps and side walls of the target cell. They consist mostly of residual nitrogen and oxygen still present in the scattering chamber in spite of the good vacuum conditions (10^{-6} mbar) [14]. The extra material affects the measured spectra and thus needs to be included in the simulation. This requires knowing the amount of cryogenic deposits at the target walls. The thickness of the depositions on the target entrance window was determined using the nitrogen/oxygen elastic data. Since this wall is exposed to the electron beam, the electrons scattered from the cryogens enter the physics spectra and can be monitored. For this purpose spectrometer A was positioned such that the nitrogen/oxygen elastic lines were inside its acceptance. The collected spectra, together with the known elastic cross-sections for these elements were used to determine the thickness of the deposited layer. On the other hand, incident

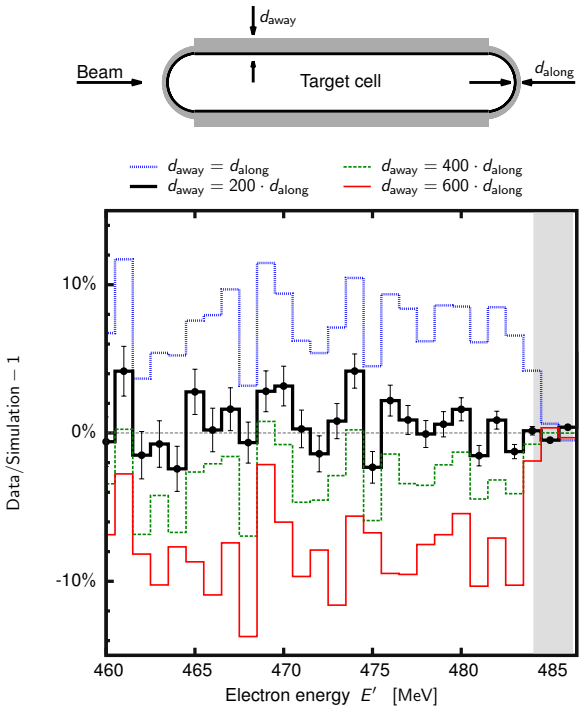

Figure 2: Top: Due to the imperfect vacuum conditions inside the scattering chamber, the residual molecules of nitrogen and oxygen gather on top of the cold target, forming a thin film of cryogenic depositions. The thickness of the layer on the side walls (d_{away}) is much thicker than the layer on the end caps (d_{along}) exposed to the beam. Bottom: Relative differences between the data and simulations for the first experimental setup at 495 MeV, including data at the elastic peak and first part of the radiative tail. The blue line shows the original comparison considered in [10], when the simulation assumes a uniform layer of cryogens around the target cell. The inconsistency between the data and simulation, which affects the trend of the ratio in the first 5 MeV of the radiative tail is evidence that the layer of cryogens away from the beam is significantly thicker than along the beam. The black, green and red line demonstrate the ratios, when the layer on the side walls is 200-, 400- and 600-times thicker than on the end caps. For the 495 MeV setting the analysis determined the best ratio to be 180 ± 10. The systematic uncertainty of all the points is 0.5 %. The grey band marks the position and width of the elastic line inside the spectrometer acceptance.

electrons do not scatter from the material on the side walls, hence the cryogens there are not directly detectable by the spectrometers. Furthermore, depositions on the side walls can be much thicker than those on the end caps, because the former are not heated by the electron beam. The amount of cryogens there was estimated by matching the functional dependence of the simulation to the measured elastic spectra, which is uniquely correlated to the thickness of the traversed material. See Fig. 2. The analysis has showed that the layer of cryogens on the side can be as much as 200 times thicker (roughly $4 \cdot 10^{-3}$ g/cm^2) than at the end caps.

With this advancement the agreement between the data and simulation improved significantly and allowed us to include the elastic data in the new analysis presented in this paper. Following the approach described in [10] the full set of 25 data points could then be used to extract the proton-charge form factors for $0.001 \leq Q^2 \leq 0.017\,\mathrm{GeV}^2/c^2$. The values and the details of the extraction have been presented in [15].

3. Experimental uncertainties

Although the ISR experiment provides remarkable control over the systematic uncertainties, a few ambiguities remain and limit the precision of the results [10]. The contributions relevant for the extraction of the proton charge radius include the uncertainty in the relative luminosity (0.17 %), the uncertainty in the detector efficiencies (0.2 %) and the contamination coming from the target support frame and the spectrometer entrance flange (0.4 %). The uncertainty of the elastic data associated with the contamination of the spectra with the cryogenic depositions is 0.24 %. The portion of the spectrum containing contributions from the pion electroproduction is 0.5 %, but is significant only for the 495 MeV setting. The combined pointwise systematic uncertainties are presented in Fig. 4.

4. Parameterisation of the form factor

For $Q^2 < 0.02\,\mathrm{GeV}^2/c^2$, it suffices for all practical purposes to parameterise the measured proton charge form-factor by using a polynomial of the form

$$G(Q^2) = n_{E_0}\left[1 - \frac{r_p^2\,Q^2}{6\,\hbar^2} + \frac{a\,Q^4}{120\,\hbar^4} - \frac{b\,Q^6}{5040\,\hbar^6}\right], \qquad (2)$$

where n_{E_0} represents the normalisation of the data, r_p represents the radius and the higher moments a and b determine the curvature of the model. Although the Q^4- and Q^6-terms at $Q^2 < 0.02\,\mathrm{GeV}^2/c^2$ account for only about a percent of the form factor value, they need to be considered in the fit. Due to a strong correlation between radius and a (b) which was estimated to be 0.97 (0.92), a wrong choice of these parameters could shift the value of the radius at the level of 0.01(0.003) fm, see Fig. 3. Data in the available Q^2 range (even with a superior experimental precision) do not permit simultaneous determination of all three parameters [16]. Therefore, a and b need to be taken from the literature. To minimise the bias of the extracted radius, we considered values obtained from the analysis of the available world data [17] which are consistent with the latest experimental results from Jefferson Lab [5]:

$$a = (2.59 \pm 0.194)\,\mathrm{fm}^4\,, \qquad b = (29.8 \pm 14.71)\,\mathrm{fm}^6\,.$$

5. Extraction of the radius

The prevailing way of determining the proton charge radius is by comparing the measured sets of proton-charge form factors with a selected model. Following the steps in [10] the data were fit by a polynomial (2), using common parameter for the radius, r_p, and different renormalisation factors, n_{E_0}, one for each energy. See [15] for details. In terms of this fit with 21 degrees of freedom and χ^2 of 18.3, the radius was determined to be $r_p = (0.868 \pm 0.017_{\mathrm{stat.}} \pm 0.059_{\mathrm{syst.}} \pm 0.003_{\mathrm{mod.}})\,\mathrm{fm}$. The

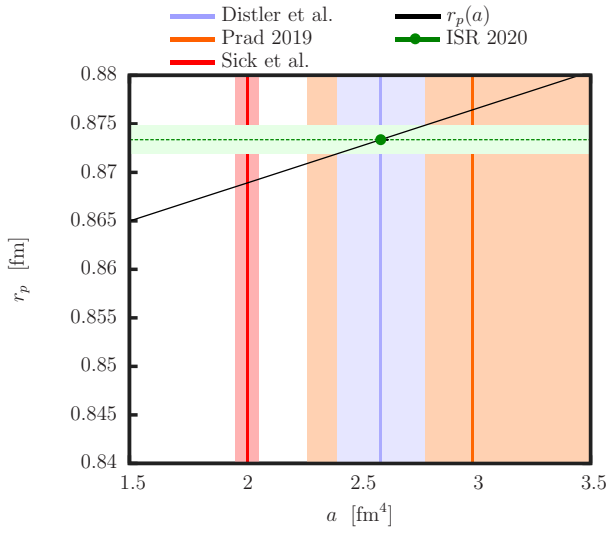

Figure 3: The proton charge radius, r_p, extracted from the data using Eq. (2), depends on the value of the parameter a in accordance with the full black line. The red line and the error band show the value of the parameter a determined by Sick et al. [16]. The orange line with the corresponding uncertainty band shows the result extracted from the most recent experiment at Jefferson Lab [5]. The blue vertical line and the corresponding uncertainty band demonstrate the value obtained by Distler et al. [17] who performed a comprehensive analysis of world data until 2010. Relying on his parameter, the green band surrounding the green dashed line denotes the model uncertainty of the radius extracted in this experiment.

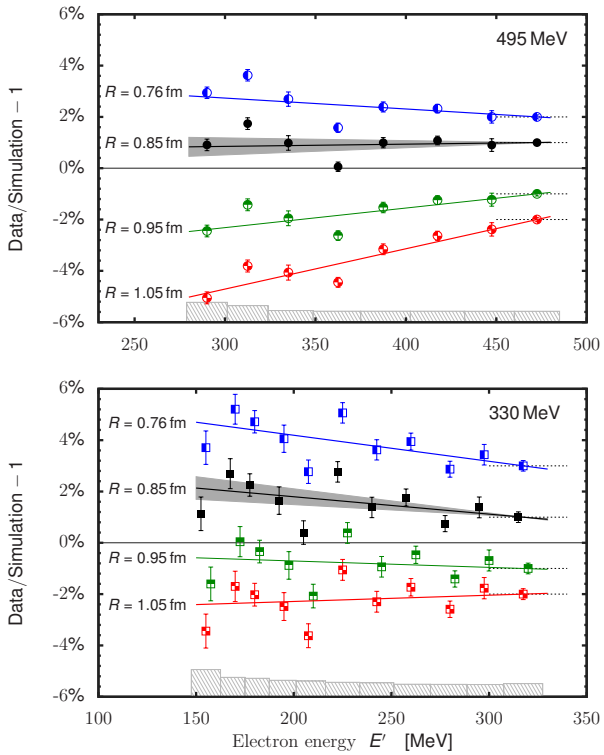

Figure 4: Relative differences between the data and simulations for 495 MeV (top) and 330 MeV (bottom) settings. Each set of ratios corresponds to simulations with a different value of the proton charge radius r_p = 0.76 fm (blue), 0.85 fm (black), 0.95 fm (green) and 1.05 fm (red). The ratios are normalised to the first (elastic) point and are artificially offset from zero (denoted by the thin dashed line) for clarity. The corresponding lines demonstrate linear fits to the data. The gray band shows the uncertainty of the extracted slope parameter $k(r_p)$. Gray boxes at the bottom of each plot demonstrate the systematic uncertainties considered in the determination of the fit paramater $k(r_p)$.

value of χ^2 has almost doubled with respect to the previous dataset [10], but this is due to the addition of three statistically very precise points at $Q^2 = 0.017\,\mathrm{GeV}^2/c^2$, $0.008\,\mathrm{GeV}^2/c^2$ and $0.003\,\mathrm{GeV}^2/c^2$. On the other hand, even by including these points and improving the analysis in the manner described above, the extracted radius remains governed by the systematic uncertainty and still critically depends on the available Q^2 range and the number of fitting parameters.

To improve the result within the scope of available data, an alternative approach was considered, applicable at the level of measured cross-sections. First, the cross-section ratios were normalised to the elastic point. To first order the E' evolution of the rescaled ratios between the data and the simulation at each energy setting depends linearly on the proton charge radius. Furthermore, since all points for a single energy configuration are strongly correlated due to the nature of the experimental approach, the effect of changing the radius appears as a change of the slope of the ratio, $k(r_p)$. Relying on the chosen model (2), the simulation was performed for different values of r_p between 0.76 fm and 1.05 fm and compared to the data. See Fig. 4. The results of the comparison for the two highest energy settings (330 MeV and 495 MeV) exhibit a clear dependence and sensitivity to small changes in the proton radius. On the other hand, the Q^2 values of the data at 195 MeV are so small that within the measured uncertainties these data alone demonstrate no detectable dependence on the radius and were thus excluded from the analysis.

The best estimate for the proton charge radius should reveal a constant ratio between the data and the simulation. The ratios presented in Fig. 4 indicate that the 495 MeV setting favours a radius of ≈ 0.84 fm, while the 330 MeV data suggest ≈ 1.0 fm. Finding the r_p at which the simulation matches the data corresponds to finding a point where $k(r_p) = 0$, see Fig. 5. Please note that there is a 3σ tension between the two extracted radii. The proton charge radius that agrees with both data sets corresponds to the weighted average of the results for the two beam energies, and was determined to be:

$$r_p = \left(0.873 \pm 0.011_{\mathrm{stat.}} \pm 0.025_{\mathrm{sys.}} \pm 0.002_{\mathrm{mod.}}\right)\,\mathrm{fm}\,.$$

Following this approach, the radius is the only free parameter. By investigating the slopes, the normalisations n_{E_0} disappear from the analysis, resulting in a more robust extraction of the radius. The uncertainty of the radius directly follows from the uncertainties of $k(r_p)$ shown in Figs. 4 and 5 . The statistical uncertainty combines contributions of data and simulation, added in quadrature. The number of simulated events was chosen such that the simulated uncertainty is always smaller then the experimental one. The systematic uncertainty is dominated by the point-like contributions presented in Sec. 3. The model dependent uncertainty is dominated by the uncertainty of the

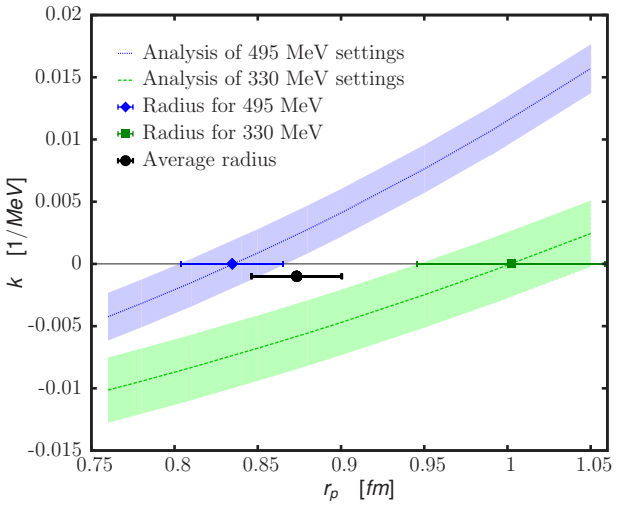

Figure 5: The ratio between the data and simulation shown in Fig. 4 depends linearly on the energy of the scattered electron, E'. The slope parameter describing this linear trend, k, depends on the r_p considered in the simulation. This figure shows how $k(r_p)$ changes with the radius for the 495 MeV (blue) and 330 MeV (green) settings. The surrounding error bands denote the uncertainty of the slope parameter $k(r_p)$, see also Fig. 4. The point where the curve crosses zero represents a radius where the simulation best matches the data. The blue and green point (together with the corresponding uncertainties) show the best radii for the two analysed data sets. The black point represents their weighted average.

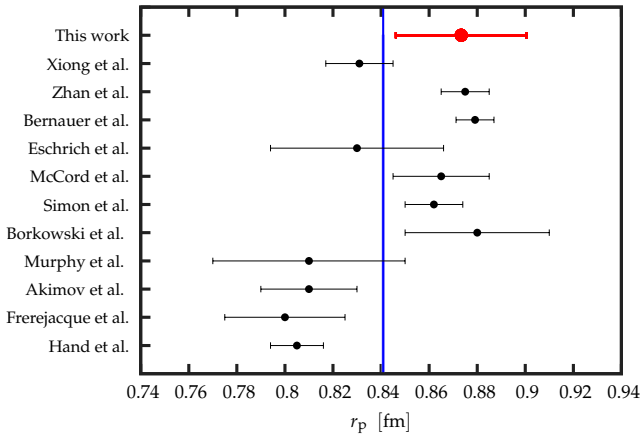

Figure 6: The proton charge radius extracted from the ISR experiment together with previous electron scattering measurements [5, 18–27]. The value obtained from the Lamb shift measurements in muonic hydrogen is shown by the blue line for the comparison.

parameter a considered in (2) to model G_E^p in the simulation, see Fig. 3.

6. Conclusions

The initial state radiation experiment at MAMI [10] established a new method for precise investigations of the electromagnetic structure of the nucleon and underlying electromagnetic processes at extremely small Q^2. In this paper we present our findings on the improved data analysis, which revealed the necessity of a complete consideration of cryogens deposited on the liquid hydrogen cell and their influence on the e-p scattering results. The analysis also demonstrated the precision with which these effects could be studied and offered new, improved values of the G_E^p not accessible in the original work. Furthermore, by studying the slopes of the measured radiative tails relative to the simulated ones, an alternative approach for the extraction of the proton charge radius was developed, which yielded a competitive new value (see Fig. 6) and almost tripled the precision of our initial result [10].

Acknowledgments

The authors would like to thank the MAMI accelerator group for the excellent beam quality which made this experiment possible. This work is supported by the Federal State of Rhineland-Palatinate, by the Deutsche Forschungsgemeinschaft with the Collaborative Research Center 1044, by the Slovenian Research Agency under Grant Z1-7305, by Croatian Science Foundation under the project IP-2018-01-8570 and U. S. Department of Energy under Award Numbers DE-FG02-96ER41003 and DE-FG02-94ER40818.

References

[1] R. Pohl, et al., The size of the proton, Nature 466 (2010) 213–216.
[2] A. Antognini, et al., Proton structure from the measurement of 2s-2p transition frequencies of muonic hydrogen, Science 339 (2013) 417–420. doi:10.1126/science.1230016.
[3] P. J. Mohr, D. B. Newell, B. N. Taylor, Codata recommended values of the fundamental physical constants: 2014, Rev. Mod. Phys. 88 (2016) 035009. doi:10.1103/RevModPhys.88.035009.
[4] A. Beyer, L. Maisenbacher, A. Matveev, R. Pohl, K. Khabarova, A. Grinin, T. Lamour, D. C. Yost, T. W. Hänsch, N. Kolachevsky, T. Udem, The rydberg constant and proton size from atomic hydrogen, Science 358 (2017) 79–85. arXiv:http://science.sciencemag.org/content/358/6359/79.full.pdf, doi:10.1126/science.aah6677.
URL http://science.sciencemag.org/content/358/6359/79
[5] W. Xiong, et al., A small proton charge radius from an electron–proton scattering experiment, Nature 575 (7781) (2019) 147–150. doi:10.1038/s41586-019-1721-2.
[6] H. Fleurbaey, S. Galtier, S. Thomas, M. Bonnaud, L. Julien, F. m. c. Biraben, F. m. c. Nez, M. Abgrall, J. Guéna, New measurement of the $1s - 3s$ transition frequency of hydrogen: Contribution to the proton charge radius puzzle, Phys. Rev. Lett. 120 (2018) 183001. doi:10.1103/PhysRevLett.120.183001.
URL https://link.aps.org/doi/10.1103/PhysRevLett.120.183001
[7] R. Pohl, R. Gilman, G. A. Miller, K. Pachucki, Muonic hydrogen and the proton radius puzzle, Ann. Rev. Nucl. Part. Sci. 63 (2013) 175–204. doi:10.1146/annurev-nucl-102212-170627.
[8] C. E. Carlson, The proton radius puzzle, Prog. Part. Nucl. Phys. 82 (2015) 59–77. doi:http://dx.doi.org/10.1016/j.ppnp.2015.01.002.
[9] M. Vanderhaeghen, J. M. Friedrich, D. Lhuillier, D. Marchand, L. Van Hoorebeke, J. Van de Wiele, Qed radiative corrections to virtual compton scattering, Phys. Rev. C 62 (2000) 025501. doi:10.1103/PhysRevC.62.025501.
[10] M. Mihovilovič, et al., First measurement of proton's charge form factor at very low Q^2 with initial state radiation, Phys. Lett. B 771 (2017) 194–198. arXiv:1612.06707, doi:10.1016/j.physletb.2017.05.031.

[11] K. Blomqvist, et al., The three-spectrometer facility at the mainz microtron {MAMI}, Nucl. Instr. and Meth. A 403 (1998) 263–301. doi:http://dx.doi.org/10.1016/S0168-9002(97)01133-9.

[12] L. W. Mo, Y. S. Tsai, Radiative corrections to elastic and inelastic ep and up scattering, Rev. Mod. Phys. 41 (1969) 205–235. doi:10.1103/RevModPhys.41.205.

[13] 56 - on the energy loss of fast particles by ionisation, in: D. T. HAAR (Ed.), Collected Papers of L.D. Landau, Pergamon, 1965, pp. 417 – 424. doi:https://doi.org/10.1016/B978-0-08-010586-4.50061-4.
URL http://www.sciencedirect.com/science/article/pii/B9780080105864500614

[14] M. Mihovilovič, et al., Initial state radiation experiment at MAMI, EPJ Web Conf. 72 (2014) 00017. doi:10.1051/epjconf/20147200017.

[15] M. Mihovilovic, et al., See supplemental material for more details.

[16] I. Sick, D. Trautmann, Reexamination of proton rms radii from low-q power expansions, Phys. Rev. C 95 (2017) 012501. doi:10.1103/PhysRevC.95.012501.
URL https://link.aps.org/doi/10.1103/PhysRevC.95.012501

[17] M. O. Distler, J. C. Bernauer, T. Walcher, The {RMS} charge radius of the proton and zemach moments, Phys. Lett. B 696 (2011) 343–347. doi:http://dx.doi.org/10.1016/j.physletb.2010.12.067.

[18] L. N. Hand, D. G. Miller, R. Wilson, Electric and magnetic form factors of the nucleon, Rev. Mod. Phys. 35 (1963) 335–349. doi:10.1103/RevModPhys.35.335.
URL https://link.aps.org/doi/10.1103/RevModPhys.35.335

[19] D. Frèrejacque, D. Benaksas, D. Drickey, Proton form factors from observation of recoil protons, Phys. Rev. 141 (1966) 1308–1312. doi:10.1103/PhysRev.141.1308.
URL https://link.aps.org/doi/10.1103/PhysRev.141.1308

[20] Yu. K. Akimov, et al., Small angle scattering of electrons by protons, Sov. Phys. JETP 35 (1972) 651–654, [Zh. Eksp. Teor. Fiz. 62, 1231 (1972)].

[21] J. J. Murphy, Y. M. Shin, D. M. Skopik, Proton form factor from 0.15 to 0.79 fm^{-2}, Phys. Rev. C 9 (1974) 2125–2129. doi:10.1103/PhysRevC.9.2125.
URL https://link.aps.org/doi/10.1103/PhysRevC.9.2125

[22] F. Borkowski, G. G. Simon, V. H. Walther, R. D. Wendling, On the determination of the proton RMS-radius from electron scattering data, Z. Phys. A275 (1975) 29–31. doi:10.1007/BF01409496.

[23] G. Simon, C. Schmitt, F. Borkowski, V. Walther, Absolute electron-proton cross sections at low momentum transfer measured with a high pressure gas target system, Nucl. Phys. A 333 (1980) 381–391. doi:http://dx.doi.org/10.1016/0375-9474(80)90104-9.

[24] M. McCord, H. Crannell, L. W. Fagg, J. T. O'Brien, D. I. Sober, J. W. Lightbody, X. K. Maruyama, P. A. Treado, Preliminary results of a new determination of the rms charge radius of the proton, Nucl. Instrum. Meth. B 56-57 (1991) 496–499. doi:10.1016/0168-583X(91)96079-Z.

[25] I. Eschrich, et al., Physics Letters B 522 (2001) 233–239. doi:https://doi.org/10.1016/S0370-2693(01)01285-0, [link].
URL http://www.sciencedirect.com/science/article/pii/S0370269301012850

[26] J. C. Bernauer, et al., High-precision determination of the electric and magnetic form factors of the proton, Phys. Rev. Lett. 105 (2010) 242001. doi:10.1103/PhysRevLett.105.242001.

[27] X. Zhan, et al., High-precision measurement of the proton elastic form factor ratio at low, Physics Letters B 705 (2011) 59–64. doi:http://dx.doi.org/10.1016/j.physletb.2011.10.002.